Quantum-noise measurements of Raman amplifiers using an interferometer

R. C. Swanson, P. R. Battle, and J. L. Carlsten
Physics Department, Montana State University, Bozeman, Montana 59717
(Received 17 June 1991)

We have measured the quantum noise added to a signal by a Raman amplifier. This was done using a modified Mach-Zender interferometer with an amplifier placed in each leg. Quantum noise added by the amplifiers manifests itself by degrading the visibility of the ensemble-average output fringe patterns. The amount of noise added by the amplifiers is deduced from the degradation of the visibility. The experimental results are compared with both ideal, single-mode amplifier theory and Raman theory. We find that the Raman amplifier operates near the quantum limit with only a few input photons per mode required to dominate the noise added by the amplifiers.

PACS number(s): 42.60.Da, 42.50.Kb, 42.65.Dr

I. INTRODUCTION

The role of amplifiers in physics has been studied and discussed considerably. This is appropriate since the microscopic phenomena frequently studied emit signals that must be amplified for observation. One must then be concerned about whether the output of the amplifier yields an accurate representation of the microscopic phenomena or if it has been significantly altered during amplification.

Theoretical work has shown that bosonic linear amplifiers necessarily add quantum noise to the output signal [1–4]. (A linear amplifier is a device whose output modes are linearly related to its input modes). For the output field to satisfy the commutation relations, noise must be added during the amplification, or put another way, noise is fundamentally required by the Heisenberg uncertainty relation. For large gain the amount of noise that a linear amplifier will add to a signal will be at least what one would expect from the amplification of one quantum per mode at the input of a noiseless amplifier.

Past studies have shown that some real amplifiers can approach the minimum amount of noise required by quantum mechanics. For example, amplifiers based on dc superconducting quantum interference devices (SQUID's) [5,6] have noise characteristics that approach the quantum limit. Other experiments using laser gain tubes have shown that the measured noise power [7,8] is consistent with the quantum limit. The frequency noise in a four-frequency laser gyro has also been found to be consistent with a laser gain tube operating near the quantum limit [9]. Recent results indicate that fiber amplifiers are approaching the quantum limit [10]. In a highly sensitive projection system using both a laser gain tube and a phase-conjugating mirror, the quantum limit was approached with only five photons required per resolution element [11].

In Raman scattering a pump photon is scattered off a molecule, leaving it in an excited state and emitting a red-shifted photon, referred to as a Stokes photon. This process can occur spontaneously, or it can occur via stimulation from an input Stokes field and thus act as an amplifier of the Stokes field. Experiments in Raman scattering have tended to fit into two distinct categories: Either they rely on spontaneous Raman scattering for initiation, where there is no input signal [12,13] to amplify, or they have such a large input signal [14] that spontaneous Raman scattering (noise) is insignificant. The regime where both spontaneous emission and the input signal have a signal effect at the output of the amplifier occurs when the input signal has only a few photons per mode. Probing this regime is interesting not only because it allows one to rigorously test the full quantum theory of Raman scattering [15,16], but also because it explicitly demonstrates how good the Raman amplifier is.

In the regime of Raman scattering where both quantum noise and the input field are important, recent work studying the spatial modes of a Raman amplifier [17] has shown that approximately 30 photons per mode in the input signal are required for the input signal's spatial mode to dominate the output spatial signal for 50% of the shots. Although this experiment indicates that there is not an excessive amount of noise introduced in a Raman amplifier, a comparison of the theory with experiment appears to be difficult.

In this paper we present results from an experiment using Raman amplifiers in each leg of a modified Mach-Zender interferometer [18]. In this experiment small signals were input to the interferometer, which were then amplified within the interferometer. The quantum noise added to the signal during amplification manifested itself by degrading the ensemble-average fringe pattern from the interferometer, which was quantified by measuring the fringe visibility.

We also present theoretical calculations of the fringe visibility. For simplicity, we first do the analysis using ideal, single-mode amplifiers. This will show how the noise introduced by an amplifier degrades the visibility of the output fringe pattern with a model that can be analyzed analytically. Additionally, we show what conditions the amplifier must satisfy to minimize the number of noise photons. Following this, the analysis is extended to Raman amplifiers, with similarities between the ideal, single-mode and Raman amplifiers noted. A description of the experiment performed to measure the fringe visibility is given in Sec. III. Finally, in Sec. IV, the results of

the calculations for the ideal, single-mode and Raman amplifiers are compared with the experimental results.

II. THEORY

To study the noise added by an amplifier, we consider the experiment diagramed schematically in Fig. 1. A generator provides a signal for a Mach-Zender interferometer with amplifiers in each leg. The amplified fields from each leg of the interferometer are combined at the exit-beam splitter with a slight angle between the combined fields to produce a fringe pattern on the screen.

The output field from an amplifier can be thought to consist of a superposition of the field due to stimulated emission from the input signal along with the field due to amplified spontaneous emission [19]. As one would expect, the amplified spontaneous emission (noise) [20] from two separate amplifiers is uncorrelated in phase [21], and therefore the relative phase difference between the combined fields is random from shot to shot, leading to random positions of the peaks and troughs in the output fringe pattern. Since the peak and trough positions are random from shot to shot, the ensemble average of such fringe patterns yields a smooth profile.

On the other hand, amplification of the input signal by stimulated emission preserves the phase of the input field. Therefore, the amplified fields resulting from stimulated emission of the input signal have a well-defined phase difference between the two legs that is dependent on the interferometer. This leads to fringe patterns that are stationary from shot to shot. Thus the ensemble average of the fringe patterns due to the field from stimulated emission retains well-defined fringes.

In general, the ensemble average of the output fringe patterns will consist of a smooth profile with a fringe pattern on top [22(a)]. The fringe pattern is attributed to the amplified signal, while the smooth profile is attributed to the noise. The larger the field arising from the input signal relative to the amplifier added noise, the larger the peaks will be compared to the smooth profile. To obtain a quantitative measure of the degradation of the fringe pattern due to the amplifier added noise, we calculated the visibility V:

$$V=\frac{\langle\hat{I}\rangle_{\max}-\langle\hat{I}\rangle_{\min}}{\langle\hat{I}\rangle_{\max}+\langle\hat{I}\rangle_{\min}}, \tag{1}$$

where $\langle\hat{I}\rangle_{\max}$ is the intensity of the peak of the ensemble fringe pattern and $\langle\hat{I}\rangle_{\min}$ is the intensity of the trough of the ensemble fringe pattern. A smooth intensity profile is one where $\langle\hat{I}\rangle_{\max}=\langle\hat{I}\rangle_{\min}$ and, as can be seen from Eq. (1), has a visibility of 0. On the other extreme, a "perfect" ensemble fringe pattern is one in which $\langle\hat{I}\rangle_{\min}=0$ and $\langle\hat{I}\rangle_{\max}$ is nonzero. Such a fringe pattern has a visibility of 1. For this to happen the phase information of the input signal has to be preserved on every shot, which means that the amplified signal must completely dominate any noise added during amplification. As we will see, this limit is approached asymptotically when the input signals become large.

In the following section we will calculate the visibility using ideal, single-mode, linear amplifiers to demonstrate the technique. Following this, the technique will be extended to Raman amplifiers. In Sec. IV we will compare the predictions of both these theoretical treatments to our experimental results.

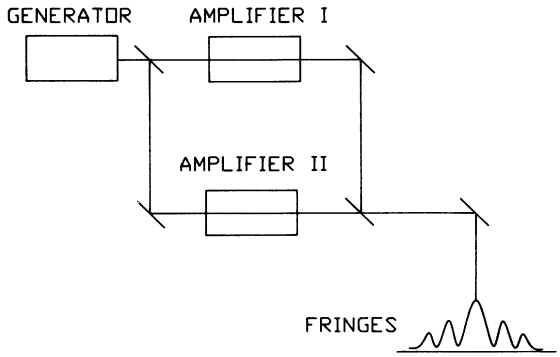

FIG. 1. Mach-Zender interferometer with an amplifier in each leg. The quantum noise added to the signal during amplification degrades the output fringe visibility.

A. Ideal, single-mode, linear amplifier

In this section we will consider an idealized amplifier whose output electric field can be expanded in some set of modes such that only one mode is significantly populated. Rather than concern ourselves with the specifics of the modes chosen, we will simply assume that the operator characteristics of this field are described by bosonic creation and annihilation operators.

With these ideal, single-mode, linear amplifiers, we will calculate the visibility of the interferometer diagramed in Fig. 1 to demonstrate the role of quantum noise in this experiment. Using a formalism similar to that presented by Caves [1], we will describe the single-mode field with creation and annihilation operators that have the free-propagation time dependence [$\exp(\pm i\omega t)$] folded out. In particular, we will choose the model where the amplifier output mode is linearly related to the input mode by

$$\hat{b}_\alpha=M_\alpha\hat{a}_\alpha+\hat{N}_\alpha\ , \tag{2}$$

where $\hat{b}_\alpha$ is the annihilation operator describing the output field of the amplifier, M_α is related to the gain of the amplifier, $\hat{a}_\alpha$ is the input-field annihilation operator, and $\hat{N}_\alpha$ is the operator governing the growth of noise in the amplifier, which depends on the amplifier internal modes. (This is not the most general form for an ideal, single-mode amplifier, but one that readily demonstrates the analysis of the interferometric method used to measure noise.) The subscript α designates the amplifiers in Fig. 1 and can take the values I, II, or G for amplifier I, amplifier II, or the generator, respectively. Note that these subscripts do not imply complete independence, for example, $[\hat{b}_{\rm I},\hat{b}^{\dagger}_{\rm II}]\neq\delta_{\rm I,II}$. We will assume that the noise field has random phase, and therefore

$$\langle\hat{N}_\alpha\rangle=0\ . \tag{3a}$$

Additionally, we assume that the internal modes of one

amplifier are independent from the internal modes of another. This assumption along with Eq. (3a) leads to

$$\langle \hat{N}_\alpha \hat{N}_\beta^\dagger \rangle = \langle \hat{N}_\alpha^\dagger \hat{N}_\beta \rangle = 0, \quad \alpha \neq \beta \tag{3b}$$

and similarly for all other combinations of the noise operator and its Hermitian adjoint for $\alpha \neq \beta$.

Since photons are bosons, the input- and output-field operators of the amplifiers must satisfy the Bose-Einstein commutation relations

$$[\hat{a}_\alpha, \hat{a}_\alpha^\dagger] = 1 , \tag{4a}$$

$$[\hat{b}_\alpha, \hat{b}_\alpha^\dagger] = 1. \tag{4b}$$

One can see that if there were not a noise term in Eq. (2), the output-field mode would not satisfy the commutation relation Eq. (4b). Combining Eqs. (2) and (4), one finds

$$[\hat{N}_\alpha, \hat{N}_\alpha^\dagger] = (1 - |M_\alpha|^2) , \tag{5}$$

where we have used the independence of the internal modes of the amplifier from the external, input-field mode.

Equation (5) provides one condition on the noise operator, but does not distinguish between low- and high-noise amplifiers. To see what condition leads to, for example, a low-noise amplifier, we calculate the expectation value of the number of photons emitted from one of these amplifiers:

$$\langle \hat{b}_\alpha^\dagger \hat{b}_\alpha \rangle = |M_\alpha|^2 \langle \hat{a}_\alpha^\dagger \hat{a}_\alpha \rangle + \langle \hat{N}_\alpha^\dagger \hat{N}_\alpha \rangle . \tag{6}$$

The first term on the right-hand side of Eq. (6) is interpreted as the amplified signal; the second is the number of amplified spontaneous emission photons or noise [20]. Rearranging Eq. (5) and inserting it into Eq. (6), one obtains

$$\langle \hat{b}_\alpha^\dagger \hat{b}_\alpha \rangle = |M_\alpha|^2 \langle \hat{a}_\alpha^\dagger \hat{a}_\alpha \rangle + \langle \hat{N}_\alpha \hat{N}_\alpha^\dagger \rangle + |M_\alpha|^2 - 1 . \tag{7}$$

The last three terms in Eq. (7) correspond to the number of noise photons emitted by the amplifier. To achieve low noise, we wish to find the condition necessary for this amplifier to emit the minimum number of noise photons allowed by quantum mechanics. Noting that $\langle \hat{N}_\alpha \hat{N}_\alpha^\dagger \rangle \geq 0$, we see that the condition for the minimum number of noise photons is

$$\langle \hat{N}_\alpha \hat{N}_\alpha^\dagger \rangle = 0 . \tag{8}$$

When this condition is satisfied and the amplifier is operated in the high-gain regime ($M_\alpha \gg 1$), one can see from Eq. (7) that the average number of output-*noise* photons is equal to the average number of output-*signal* photons when there is an average of one photon in the input signal. This is why the noise is said to be equivalent to at least one photon per mode at the input to a noiseless amplifier.

No specific operating mechanism has been indicated here to satisfy the minimum noise condition of Eq. (8), and so from this analysis it is unclear exactly what operating conditions in the amplifier are required to achieve the minimum number of noise photons. However, in the following section on Raman scattering, we will observe that an analogous condition arises and can be traced to specific operating conditions.

Now, with this model of an ideal, single-mode amplifier, we calculate the fringe visibility of the interferometer diagramed in Fig. 1 [22(b)]. To do this we start with the annihilation operator of the output field of the generator, and then follow the transformation of the operator through the interferometer to the output screen.

The output field from the generator is described by the annihilation operator $\hat{b}_G$. This field is split by the input-beam splitter to the interferometer. We will assume the reflection and transmission coefficients are constant over the bandwidth of the mode. Then the input-field operator to the upper (lower) leg of the interferometer is written $t_i \hat{b}_G$ ($r_i \hat{b}_G$), where t_i (r_i) is the transmission (reflection) coefficient of the input-beam splitter [23]. (Since we will employ normal ordering of the field operators to calculate the intensity, the vacuum-field contribution from the other port of the beam splitter does not contribute and can be ignored.)

Using Eq. (2), the output-field operator from the upper amplifier is

$$\hat{b}_{\rm I} = M_{\rm I}(t_i \hat{b}_G) + \hat{N}_{\rm I} , \tag{9}$$

and the output field from the lower amplifier is found by replacing the subscript I with II and inserting r_i for t_i. The final output-field operator $[\hat{b}_{\rm tot}(x)]$ from the interferometer can be written

$$\hat{b}_{\rm tot}(x) = r_0 \hat{b}_{\rm I} + t_0 \hat{b}_{\rm II} e^{i\phi(x)} , \tag{10}$$

where x is a transverse coordinate of the field and t_0 and r_0 are the transmission and reflection coefficients of the output-beam splitter, respectively. The phase factor $\phi(x)$ results because a small angle was placed between the combined fields at the output-beam splitter.

The intensity pattern is calculated using the quantum-mechanical expectation value for the normally ordered product:

$$\begin{aligned} \langle \hat{I}(x) \rangle &= K(\langle \hat{b}_{\rm tot}^\dagger(x) \hat{b}_{\rm tot}(x) \rangle \\ &= K(|r_0|^2 \langle \hat{b}_{\rm I}^\dagger \hat{b}_{\rm I} \rangle + |t_0|^2 \langle \hat{b}_{\rm II}^\dagger \hat{b}_{\rm II} \rangle \\ &\quad + r_0 t_0^* \langle \hat{b}_{\rm I}^\dagger \hat{b}_{\rm II} \rangle e^{i\phi(x)} + r_0^* t_0 \langle \hat{b}_{\rm II}^\dagger \hat{b}_{\rm I} \rangle e^{-i\phi(x)}) , \end{aligned} \tag{11}$$

where K keeps the units correct and may include temporal information about the pulse, but is unimportant for the discussion at hand. We assume good spatial overlap of the fields from each leg of the interferometer. In Eq. (11) one sees that replacing the complex transmission and reflection coefficients with their absolute values shifts the positions of the maximum and minimum intensity profiles along the x coordinate. Since the location of the maximum and minimum intensity profiles is unimportant in the visibility calculation, we make this simplification without affecting the results of our calculations. The expectation value for the maximum intensity is found by choosing the position where the phase is such that constructive interference results. Similarly, the minimum in-

tensity is found by choosing the position where destructive interference occurs:

$$\langle \hat{I} \rangle_{\max} = K(r_0^2 \langle \hat{b}_{\mathrm{I}}^{\dagger} \hat{b}_{\mathrm{I}} \rangle + t_0^2 \langle \hat{b}_{\mathrm{II}}^{\dagger} \hat{b}_{\mathrm{II}} \rangle + r_0 t_0 \langle \hat{b}_{\mathrm{I}}^{\dagger} \hat{b}_{\mathrm{II}} \rangle + r_0 t_0 \langle \hat{b}_{\mathrm{II}}^{\dagger} \hat{b}_{\mathrm{I}} \rangle) , \quad (12a)$$

$$\langle \hat{I} \rangle_{\min} = K(r_0^2 \langle \hat{b}_{\mathrm{I}}^{\dagger} \hat{b}_{\mathrm{I}} \rangle + t_0^2 \langle \hat{b}_{\mathrm{II}}^{\dagger} \hat{b}_{\mathrm{II}} \rangle - r_0 t_0 \langle \hat{b}_{\mathrm{I}}^{\dagger} \hat{b}_{\mathrm{II}} \rangle - r_0 t_0 \langle \hat{b}_{\mathrm{II}}^{\dagger} \hat{b}_{\mathrm{I}} \rangle) . \quad (12b)$$

The visibility is then calculated to be

$$V = \frac{r_0 t_0 r_i t_i (M_{\mathrm{I}}^* M_{\mathrm{II}} + M_{\mathrm{II}}^* M_{\mathrm{I}})(\langle \hat{b}_G^{\dagger} \hat{b}_G \rangle)}{(r_0^2 t_i^2 |M_{\mathrm{I}}|^2 + r_i^2 t_0^2 |M_{\mathrm{II}}|^2)(\langle \hat{b}_G^{\dagger} \hat{b}_G \rangle) + r_0^2 \langle \hat{N}_{\mathrm{I}}^{\dagger} \hat{N}_{\mathrm{I}} \rangle + t_0^2 \langle \hat{N}_{\mathrm{II}}^{\dagger} \hat{N}_{\mathrm{II}} \rangle} . \quad (14)$$

Note that noise terms do not appear in the numerator since terms such as $\langle \hat{N}_{\mathrm{I}}^{\dagger} \hat{N}_{\mathrm{II}} \rangle$ are zero. The noise terms are present only in the denominator where, as one would expect, they diminish the output visibility. The term $\langle \hat{b}_G^{\dagger} \hat{b}_G \rangle$ is simply the expectation value of the number of input photons to the interferometer. In Eq. (14) one can see that if zero photons are input into the interferometer, the visibility vanishes, again the result one would expect. The visibility increases as one increases the number of photons input to the interferometer because there is more signal to compete with the noise.

We consider a specific example of a balanced interferometer to observe the behavior of the visibility as a function of the number of photons input to the interferometer. To balance the interferometer, we let the gains be equal in the two amplifiers and let both the input- and output-beam splitters be equal:

$$M_{\mathrm{I}} = M_{\mathrm{II}} = M , \quad (15a)$$

$$\langle \hat{N}_{\mathrm{I}}^{\dagger} \hat{N}_{\mathrm{I}} \rangle = \langle \hat{N}_{\mathrm{II}}^{\dagger} \hat{N}_{\mathrm{II}} \rangle = \langle \hat{N}^{\dagger} \hat{N} \rangle = \langle \hat{N} \hat{N}^{\dagger} \rangle + |M|^2 - 1 , \quad (15b)$$

$$t_i = t_0 = t , \quad (15c)$$

$$r_i = r_0 = r , \quad (15d)$$

where we have again noted the result of Eq. (5) in Eq. (15b).

Inserting the above conditions into Eq. (14) leads to a simpler expression for the visibility:

$$V = \frac{\langle \hat{b}_G^{\dagger} \hat{b}_G \rangle}{\langle \hat{b}_G^{\dagger} \hat{b}_G \rangle + (1 - |M|^{-2} + \langle \hat{N} \hat{N}^{\dagger} \rangle)/2t^2 r^2} . \quad (16)$$

If the term $\langle \hat{N} \hat{N}^{\dagger} \rangle$ is large, which as we saw above indicates a noisy amplifier, then the visibility is diminished. Not surprisingly, the condition for maximum visibility from the interferometer is the same we required for minimizing the number of noise photons:

$$V = \frac{r_0 t_0 (\langle \hat{b}_{\mathrm{I}}^{\dagger} \hat{b}_{\mathrm{II}} \rangle + \langle \hat{b}_{\mathrm{II}}^{\dagger} \hat{b}_{\mathrm{I}} \rangle)}{r_0^2 \langle \hat{b}_{\mathrm{I}}^{\dagger} \hat{b}_{\mathrm{I}} \rangle + t_0^2 \langle \hat{b}_{\mathrm{II}}^{\dagger} \hat{b}_{\mathrm{II}} \rangle} . \quad (13)$$

The visibility is large when the cross correlation between the two amplified fields is large and is small when the cross correlation is small relative to the correlation of the output fields of the amplifiers with themselves. This is what one expects since only the input signal will sample both legs of the interferometer and can contribute to the cross correlation between the two amplified fields.

To see the effects of the amplifier noise, we substitute Eq. (9) into Eq. (13). Using Eqs. (3) and the fact that the noise operator is independent of the input-field mode, the following form for the visibility is found:

$$\langle \hat{N} \hat{N}^{\dagger} \rangle = 0 . \quad (17)$$

If one chooses a single-mode amplifier with the minimum noise requirement of Eq. (17), uses beam splitters with 50:50 transmission-to-reflection ratios, and goes to high gain (i.e., $|M|^2 \gg 1$), the visibility expression reduces to the simple form

$$V = \frac{\langle \hat{b}_G^{\dagger} \hat{b}_G \rangle}{\langle \hat{b}_G^{\dagger} \hat{b}_G \rangle + 2} . \quad (18)$$

Note that with two photons input to the interferometer (and therefore an average of one photon to each amplifier), the visibility is 0.5. The visibility as a function of the average number of photons input to each amplifier is shown in Fig. 2. This plot shows that even with an input signal of only eight photons (or four photons on average per amplifier), the output visibility is 0.8, indicating

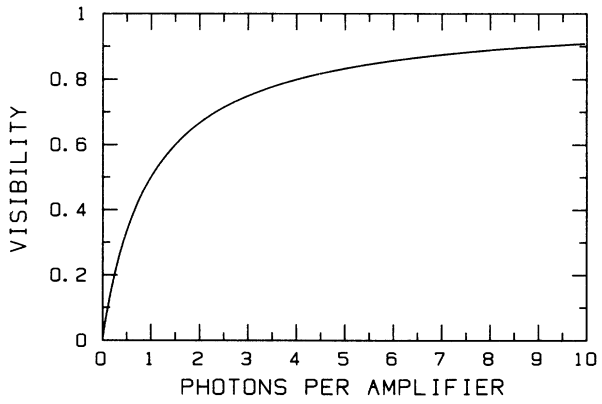

FIG. 2. Theoretical visibility from the interferometer shown in Fig. 1 with ideal, single-mode amplifiers. The horizontal axis indicates how many photons on average are input to each amplifier. Note that very few photons are required to achieve high visibility.

that the noise can be dominated with quite small inputs.

In the next section we apply the formalism used above to the more complicated situation using Raman amplifiers.

B. Raman scattering

Now we replace the ideal, single-mode, linear amplifiers in Fig. 1 with Raman amplifiers and repeat the analysis. This analysis will show that the procedure used above works on a real system and, in fact, is essentially the same. To treat this problem we will employ the fully quantum-mechanical model of Raman scattering [16,24]. This plane-wave model assumes that a pencil-shaped region of a Raman-active medium is pumped with a large classical field. Additionally, the pump laser is assumed to remain undepleted as it passes through the Raman medium. The slowly varying, negative-frequency Stokes-field operator is written

$$\hat{E}_{\alpha}^{(-)}(z,\tau)=\hat{E}_{\alpha}^{(-)}(0,\tau)+\int_0^{\tau}d\tau'\,\hat{E}_{\alpha}^{(-)}(0,\tau')B_{\alpha}(z,\tau,\tau') +\hat{N}_{\alpha}^{\dagger}(z,\tau)\ , \tag{19}$$

where $\hat{E}_{\alpha}^{(-)}(z,\tau)$ is the field operator at position z in the Raman cell and at retarded time $\tau=t-z/c$, $\hat{E}_{\alpha}^{(-)}(0,\tau)$ is the input Stokes-field operator to the Raman cell, and $\hat{N}_{\alpha}^{\dagger}(z,\tau)$ is the noise operator that is independent of the input-field operator. The exact expressions for the noise operator $\hat{N}_{\alpha}^{\dagger}(z,\tau)$ and the kernel $B_{\alpha}(z,\tau,\tau')$ are not important for the immediate discussion; however, they are given in the Appendix. As in the example with ideal, single-mode amplifiers, the subscript α can take the values I, II, and G to designate amplifier I in the interferometer, amplifier II, and the generator, respectively.

Before proceeding, we pause to note the similarities of Eq. (19) for the Raman system and Eq. (2) for the ideal, single-mode amplifier discussed above. The output-field operator $\hat{E}_{\alpha}^{(-)}(z,\tau)$ is analogous to $\hat{b}_{\alpha}^{\dagger}$. Similarly, $\hat{E}_{\alpha}^{(-)}(0,\tau)$, the Stokes field at $z=0$, is analogous to $\hat{a}_{\alpha}^{\dagger}$ as the input-field operator. There is also a clear analogy between the noise operators for the ideal, single-mode amplifier in Eq. (2), $\hat{N}_{\alpha}^{\dagger}$, and the noise operator in the Stokes field in Eq. (19), $\hat{N}_{\alpha}^{\dagger}(z,\tau)$. Also, like the ideal, single-mode amplifier, the Raman Stokes-field equation satisfies bosonic commutation relations [25]. So, as with the ideal, single-mode amplifier, the quantum noise added by the Raman amplifier is required by the commutation relations and the Raman amplifier can be thought of as a quantum-limited amplifier. With these similarities it should not be surprising to find that the analysis using Raman amplifiers closely follows the procedures above.

It is interesting to note that the antinormally ordered noise-operator correlation function is (see Appendix)

$$\langle \hat{N}_{\alpha}(z,\tau)\hat{N}_{\beta}^{\dagger}(z',\tau')\rangle=0 \tag{20}$$

for all values of the variables. For the ideal, single-mode amplifier, we found that this was the condition that led to the minimum number of noise photons; thus one would also expect that the Raman amplifier would emit the minimum number of noise photons.

With the Raman system, however, we know the operating conditions of the amplifier and can gain an understanding of why the Raman amplifier should emit the minimum number of noise photons. The result of Eq. (20) is dependent on the condition that the Raman system remains primarily in its ground state. A molecule that participates in Raman scattering is initially in its ground state and, after the two-photon Raman-scattering process, it is left in an excited state. Thus the condition that the Raman system remains primarily in its ground state means that very few molecules of the active medium are in the final state after the emission of the Stokes photon.

One can get a physical understanding of why the noise is low in an amplifier that has nearly all of its molecules in the state that is "ready" to emit photons rather than in the final state the molecules are in after emission of a photon by considering a two-level system that has a population in both states. In a two-level system the upper state is "ready" to emit a photon and the ground state is the final state after emission of a photon. With more molecules in the upper state than in the lower state, an input-signal photon at the transition frequency is more likely to amplify via stimulated emission than to be absorbed, a necessary condition for amplification. However, any signal photons that are absorbed by molecules in the lower state are potentially lost from the signal. Therefore, one would expect that the fewer molecules in the lower state (i.e., molecules that are available to absorb the photons of interest), the less noise the amplifier will emit. One then expects that the lowest-noise characteristics will be achieved when the system is completely inverted so that no molecules are in the final state of the amplifier transition [26].

Since the Raman amplifier we consider is assumed to have insignificantly few molecules in the final state of the amplifier transition, one expects that the minimum number of noise photons will be emitted.

Now, with this model of stimulated Raman scattering, we proceed to calculate the expected fringe visibility for the apparatus shown in Fig. 1 following a routine very similar to the one used in the previous section. Note that it is assumed that the input field to the Raman generator is the vacuum field, which does not contribute when the field operators are normally ordered. Similarly, the vacuum-field input at the beam splitter does not contribute in normal ordering, and so it will be ignored.

The output field of the Raman generator is written $\hat{E}_{G}^{(-)}(L_G,\tau)$, where L_G is the length of the Raman generator. Assuming that the beam-splitter coefficients are constant over the Raman linewidth, the input field to the upper (lower) amplifier in Fig. 1 is $t_i\hat{E}_{G}^{(-)}(L_G,\tau)$ [$r_i\hat{E}_{G}^{(-)}(L_G,\tau)$], where t_i (r_i) is the transmission (reflection) coefficient of the input-beam splitter. Using Eq. (19), the output field from the upper amplifier is

$$\hat{E}_{\mathrm{I}}^{(-)}(L,\tau)=t_i\hat{E}_{G}^{(-)}(L_G,\tau) +\int_0^{\tau}d\tau'\,t_i\hat{E}_{G}^{(-)}(L_G,\tau')B_{\mathrm{I}}(L,\tau,\tau') +\hat{N}_{\mathrm{I}}^{\dagger}(L,\tau)\ , \tag{21}$$

where L is the length of the Raman amplifiers (assumed

to be identical in length). The output field from the lower amplifier in Fig. 1 is the same as Eq. (21) with I's changed to II's and t_i's changed to r_i's.

The output fields from the two amplifiers combine at the exit-beam splitter to give

$$\hat{E}_{\rm tot}^{(-)}(x,\tau)=r_0\hat{E}_{\rm I}^{(-)}(L,\tau)+t_0\hat{E}_{\rm II}^{(-)}(L,\tau)e^{i\phi(x)} . \tag{22}$$

Here t_0 (r_0) is the transmission (reflection) coefficient of the exit-beam splitter of the interferometer. As in the analysis above for the single-mode amplifier, the output field is now a function of the transverse coordinate x because the beams have been combined with a slight angle between them.

The intensity pattern in units of photons per second emitted from the pumped pencil-shaped region of Raman medium can now be calculated using the normally ordered product:

$$\begin{aligned}\langle\hat{I}(x,\tau)\rangle&=\frac{Ac}{2\pi\hbar\omega_S}\langle\hat{E}_{\rm tot}^{(-)}(x,\tau)\hat{E}_{\rm tot}^{(+)}(x,\tau)\rangle\\&=\frac{Ac}{2\pi\hbar\omega_S}[|r_0|^2\langle\hat{E}_{\rm I}^{(-)}(L,\tau)\hat{E}_{\rm I}^{(+)}(L,\tau)\rangle+|t_0|^2\langle\hat{E}_{\rm II}^{(-)}(L,\tau)\hat{E}_{\rm II}^{(+)}(L,\tau)\rangle\\&\quad+r_0t_0^*\langle\hat{E}_{\rm I}^{(-)}(L,\tau)\hat{E}_{\rm II}^{(+)}(L,\tau)\rangle e^{-i\phi(x)}+r_0^*t_0\langle\hat{E}_{\rm II}^{(-)}(L,\tau)\hat{E}_{\rm I}^{(+)}(L,\tau)\rangle e^{i\phi(x)}] ,\end{aligned} \tag{23}$$

where c is the speed of light and $\hbar\omega_S$ is the energy of a Stokes photon. Since replacing the complex transmission and reflection coefficients with their absolute values leads only to an unimportant shift of the fringe pattern along the x coordinate, we make this simplification. The quantum-mechanical expectation values for the maximum and minimum intensities are then found to be

$$\begin{aligned}\langle\hat{I}(\tau)\rangle_{\rm max}&=\frac{Ac}{2\pi\hbar\omega_S}[r_0^2\langle\hat{E}_{\rm I}^{(-)}(L,\tau)\hat{E}_{\rm I}^{(+)}(L,\tau)\rangle+t_0^2\langle\hat{E}_{\rm II}^{(-)}(L,\tau)\hat{E}_{\rm II}^{(+)}(L,\tau)\rangle\\&\quad+r_0t_0\langle\hat{E}_{\rm I}^{(-)}(L,\tau)\hat{E}_{\rm II}^{(+)}(L,\tau)\rangle+t_0r_0\langle\hat{E}_{\rm II}^{(-)}(L,\tau)\hat{E}_{\rm I}^{(+)}(L,\tau)\rangle] ,\end{aligned} \tag{24a}$$

$$\begin{aligned}\langle\hat{I}(\tau)\rangle_{\rm min}&=\frac{Ac}{2\pi\hbar\omega_S}[r_0^2\langle\hat{E}_{\rm I}^{(-)}(L,\tau)\hat{E}_{\rm I}^{(+)}(L,\tau)\rangle+t_0^2\langle\hat{E}_{\rm II}^{(-)}(L,\tau)\hat{E}_{\rm II}^{(+)}(L,\tau)\rangle\\&\quad-r_0t_0\langle\hat{E}_{\rm I}^{(-)}(L,\tau)\hat{E}_{\rm II}^{(+)}(L,\tau)\rangle-t_0r_0\langle\hat{E}_{\rm II}^{(-)}(L,\tau)\hat{E}_{\rm I}^{(+)}(L,\tau)\rangle] .\end{aligned} \tag{24b}$$

Note the similarity between Eqs. (24) and (12) in the ideal, linear amplifier section.

From our experiment the fringe pattern from the interferometer was imaged onto a linear diode array. The diodes in the array integrated the intensity over the duration of the pulse. Therefore, to obtain theoretical predictions appropriate for the experiment, Eqs. (24) were integrated over the pulse. Consequently, the expression for the visibility $V_{\rm pulse}$ can be written

$$V_{\rm pulse}=\frac{\int_{\rm pulse}\langle\hat{I}(\tau)\rangle_{\rm max}d\tau-\int_{\rm pulse}\langle\hat{I}(\tau)\rangle_{\rm min}d\tau}{\int_{\rm pulse}\langle\hat{I}(\tau)\rangle_{\rm max}+\int_{\rm pulse}\langle\hat{I}(\tau)\rangle_{\rm min}d\tau} . \tag{25}$$

Note that Eq. (25) is similar to Eq. (1) except that the effects of the pulse duration are now included.

Thus using the "real" Raman amplifiers in the experimental setup diagramed in Fig. 1 is very similar to using ideal, single-mode amplifiers. To find quantitative values for the visibility, numerous integrals had to be evaluated. Additionally, we were particularly interested in the slightly different experimental setup shown in Fig. 3. The only changes that were needed to calculate the expected visibility from the interferometer shown in Fig. 3 were the inclusion of more beam splitters, which was straightforward and is discussed in the Appendix. In the next section we describe the experimental details of the fringe-visibility experiment diagramed in Fig. 3. The comparison of the theoretical and experimental results are presented in Sec. IV.

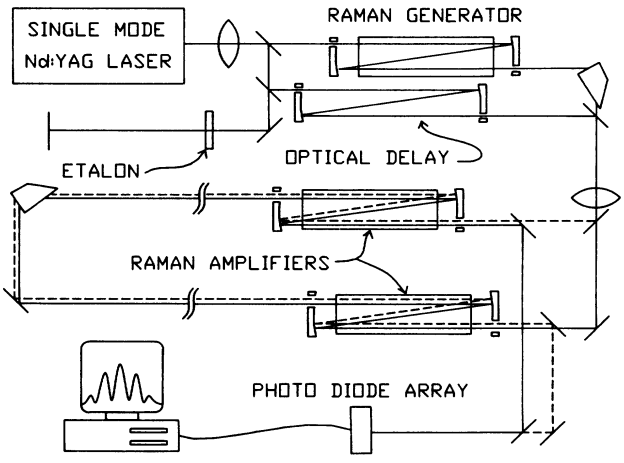

FIG 3. Nearly cyclic interferometer with a Raman amplifier in each leg. One path in the interferometer is shown with a dashed line, the other solid. The output fringe patterns are imaged onto a linear photodiode array with 25-μm resolution for data collection.

III. EXPERIMENT

In this section we describe the experiment performed to measure the output visibility from an interferometer. The experimental apparatus is diagramed in Fig. 3. Before proceeding into the details, one should note that the experimental apparatus diagramed in Fig. 3 is essentially the same as the Mach-Zender interferometer shown in Fig. 1. A generator provides a signal to an interferometer with amplifiers in each leg. The output fringes are imaged onto a linear diode array for data collection. The only difference from Fig. 1 is that in Fig. 3 the interferometer has a cyclic geometry for improved stability over the standard Mach-Zender interferometer.

With this in mind, we proceed with a detailed description of the experiment diagramed in Fig. 3. A pulsed, near-single-mode, frequency-doubled Nd:YAG laser (532 nm) with a 21.6-ns full width at half maximum Gaussian temporal profile was used to pump the Raman amplifiers. The Raman scattering was done in 10 atm of H_2 on the vibrational $Q_{01}(1)$ transition at room temperature. For this system the dephasing time for the Raman medium was $1/\Gamma=0.7$ ns [27], considerably shorter than the pump duration, which meant that collisional effects were important.

An étalon was used to monitor the pump-laser stability to ensure that no mode hops occurred during data collection. Additionally, an energy meter that was interfaced to a computer (not shown in Fig. 3) provided energy measurements of every pump-laser shot. The output Stokes signal that was input to the interferometer was varied by placing pump attenuators in front of the Raman generator (not shown in Fig. 3).

After the pulse exited the generator, the residual pump was removed from the beam with a modified Pellenbroca prism, and then additional pump energy needed for the amplification in the interferometer was added to the beam. No temporal delay was introduced between the Stokes pulse and new pump pulse. The optics necessary for beam manipulation between the generator and interferometer transmitted approximately 68% of the Stokes signal.

To achieve equal gain in the two amplifiers, the input-beam splitter to the interferometer had a 50:50 transmission-to-reflection ratio at the pump wavelength to within a percent. The pump intensity input to the amplifiers was always large enough to achieve high gain (the signal was amplified by approximately ten orders of magnitude for small input signals), but not so large as to lead to pump depletion.

Both the input- and exit-beam splitters of the interferometer had a 78:22 transmission-to-reflection ratio at the Stokes wavelength (680 nm). For the total output field of the interferometer to obtain equal contributions of amplified signal from each leg, the Stokes field that was transmitted (reflected) as it entered the interferometer was reflected (transmitted) at the exit-beam splitter.

In the near-cyclic design of the interferometer shown in Fig. 3, most of the optics in the interferometer were common to both beam paths. Consequently, slight shifts in the optics positions affected both beam paths identically and therefore did not affect the relative phase between the two beams. The cyclic design greatly increased the stability of the interferometer, which was critical since the beams traversed approximately 70 m in each leg of the interferometer. One beam path is shown as a dashed line in Fig. 3 to differentiate it from the other. Note that each beam was amplified in a separate Raman amplifier placed in a multipass cell. The multipass cells limit the amplification to a single spatial mode. After the beam was amplified, it encountered a modified Pellenbroca prism before entering a second amplifier. This removed the residual pump energy from the pulse so that no additional amplification occurred in the second amplifier. To ensure that the amplification of the two pulses was independent, the beam path between the two amplifiers was made long enough that the two pulses never overlapped inside an amplifier. The residual pump beams removed from the beam by the modified Pellenbroca prism were monitored with fast photodiodes (not shown in Fig. 3) to make certain that no pump depletion occurred during amplification.

For additional beam manipulation at the expense of only a slight loss of stability, identical "pickoff" beam splitters were used. These optics had transmission-to-reflection coefficients ratio of 50:50 at the Stokes wavelength and mark the ends of the cyclic region of the interferometer in Fig. 3.

The output fringe patterns were imaged onto a linear photodiode array with 25-μm resolution that was interfaced to a computer, allowing the fringe pattern from every shot to be recorded. Ensembles of these fringe patterns could then be formed and the resulting visibility measured.

The visibility of the ensemble fringe pattern is a function of the input signal, which is dependent on the pump-field input to the Raman generator. To clarify the significance of our results, we used the quantum-mechanical theory of stimulated Raman scattering [16] to calculate the number of photons emitted from the Raman generator for various input pump energies.

Then, including the effects of the transmission of the optics between the Raman generator and interferometer (68% transmission) and the two beam splitters a beam encounters before reaching an amplifier [28], the average number of photons reaching an amplifier was calculated. Finally, we estimated the number of Stokes temporal modes that had a significant population of photons to be the ratio of the pump linewidth to the Stokes-gain-narrowed linewidth. Because of gain narrowing [29], this ratio becomes smaller at large gains in the generator. For example, the ratio ranges from 22.3 for spontaneous Raman scattering at extremely low gain to around 4 at large gains. In this manner the input signal was transformed to units of number of input photons per mode per amplifier.

IV. RESULTS AND CONCLUSIONS

In Fig. 4 we present the ensemble average of 284 fringe patterns when no input Stokes signal was put into the interferometer. As one would expect, there is no well-

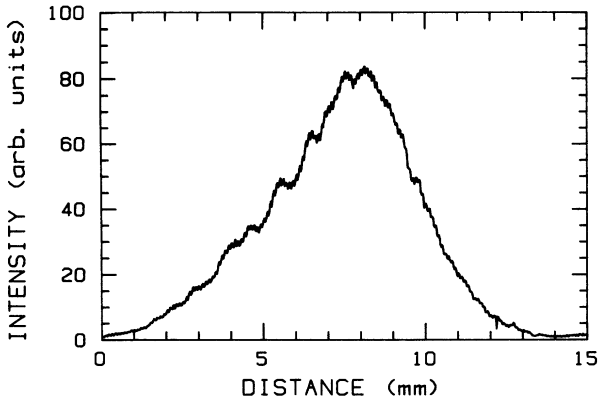

FIG. 4. Ensemble average of 284 fringe patterns when no input signals were input to the interferometer. This fringe pattern is washed out since the two output fields from the interferometer are uncorrelated. The measured visibility is 0.06.

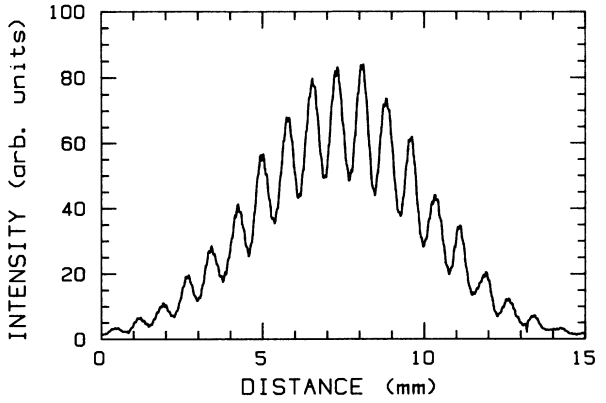

FIG. 6. With an average of 0.59 photons per mode input into each amplifier, the ensemble-average fringe pattern has a visibility of 0.30. There were 644 shots included in this ensemble.

defined fringe pattern. However, as the input signal to the interferometer is increased, the fringe pattern develops. For example, in Fig. 5 an ensemble of 832 fringe patterns with an average of 0.13 photons per mode per amplifier shows well-defined fringes on top of a smooth background. As noted above, the fringe pattern can be thought to arise from the stimulated signal, and the smooth background is the result of amplified noise in the amplifiers.

As the input signal is increased further, the amplified signal becomes more dominant, as shown in Fig. 6 with an input of 0.59 photons per mode per amplifier and Fig. 7 with an input of over 100 photons per mode per amplifier where the noise is quite well dominated.

The measured visibility of Fig. 4, which consists entirely of noise, is nearly zero ($V=0.06$). The visibility of the fringe pattern in Fig. 7 where the noise is quite well dominated approaches 1 ($V=0.95$). The effect of the Gaussian envelope has been folded out of the visibility measurements. These plots demonstrate how the output visibility is quantitatively related to the relative amount of noise in the output pulses of the amplifiers.

Figure 8 shows the experimentally measured visibility (X's) as a function of the average number of photons per mode input to the amplifiers. The solid curve in Fig. 8 represents the theoretical results from Raman theory. For comparison, the results for the same interferometer using ideal, single-mode amplifiers in place of the Raman amplifiers are shown as a dashed line. Note the similarity between the results when using ideal, single-mode amplifiers and the results when using Raman amplifiers. As one would expect, the visibility goes up as the number of photons per mode input to the amplifiers increases.

One may note that the experimentally measured visibility in Fig. 8 appears to rise more steeply than the theory. This may be due to slight variations in the pump temporal width that occurred during the data collection.

Additionally, the experimental data appear to approach asymptotically a maximum visibility somewhat lower than what theory predicts, which could be caused

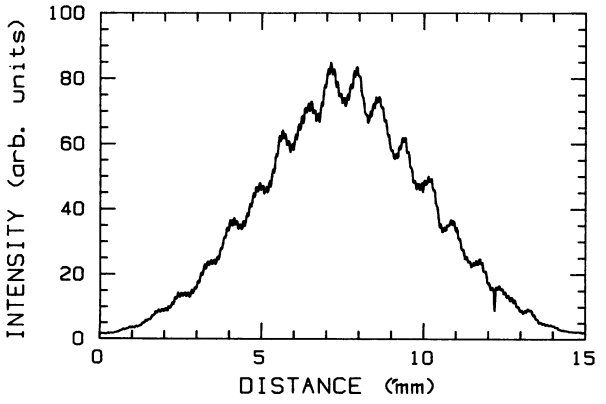

FIG. 5. Small fringes are visible on this ensemble of 832 shots with an average of 0.13 photons per mode input into each amplifier. The measured visibility of the ensemble average was 0.09.

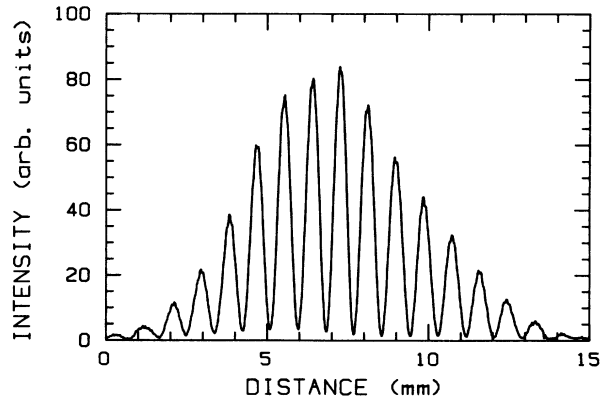

FIG. 7. Quantum noise is almost completely dominated, as shown by the deep fringe pattern. Over 100 photons per mode were input into each amplifier on average, resulting in a measured visibility of 0.95. There were 188 shots included in this ensemble.

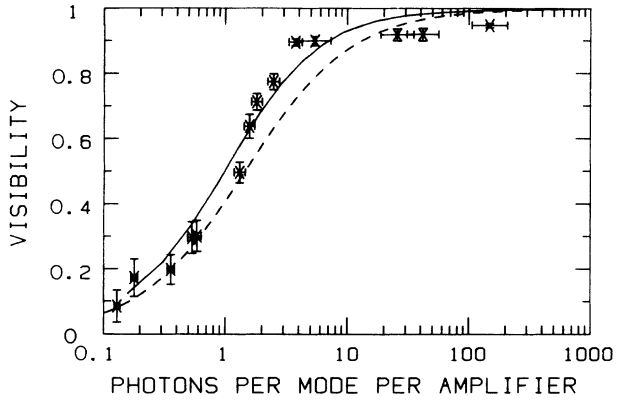

FIG. 8. Visibility as a function of the average number of photons per mode in each amplifier in the interferometer shown in Fig. 3. The ×'s indicate experimentally measured points, the solid line shows results from Raman-scattering theory, and the dashed line indicates the results one would expect if ideal, single-mode amplifiers were used. Note that very few photons are needed in each amplifier to achieve good visibility.

by an imbalance in the interferometer. To test the interferometer we periodically measured the visibility with no pump supplied to the amplifiers, thus making the amplifiers passive. These measurements yielded an average visibility of 0.96, very near the asymptotic value the experimental data appear to approach.

In conclusion, the above data indicate that the noise added in Raman amplification is in agreement with what is predicted theoretically by the theory of Raymer and Mostowski [16]. Since the noise emitted by the amplifiers is fundamentally required by the Heisenberg uncertainty relation, the Raman amplifier is an example of a quantum-mechanically limited linear amplifier. And finally, the interferometric method outlined above is a practical method to measure the noise characteristics of light amplifiers, providing easily interpretable results.

ACKNOWLEDGMENT

This work was supported by the National Science Foundation Grant No. PHY-8900282.

APPENDIX

In this appendix we give the complete expression for the Stokes-field operator equation as well as the needed expectation values of operator products that arise in the analysis. Additionally, the expression used to calculate the visibility of the experiment diagramed in Fig. 3 is presented. Finally, we provide details not given in the text necessary to duplicate our results.

The full expression for the Stokes-field operator equation is [16,24]

$$\hat{E}_\alpha^{(-)}(z,\tau)=\hat{E}_\alpha^{(-)}(0,\tau)+\int_0^z dz'\,\hat{Q}_\alpha^\dagger(z',0)A_\alpha(z,z',\tau)+\int_0^\tau d\tau'\,\hat{E}_\alpha^{(-)}(0,\tau')B_\alpha(z,\tau,\tau') + \int_0^\tau\int_0^z dz'\,d\tau'\,\hat{F}_\alpha^\dagger(z',\tau')C_\alpha(z,z',\tau,\tau')\ , \tag{A1}$$

where $\hat{E}_\alpha^{(-)}(z,\tau)$ is the negative-frequency field operator at position z in the Raman cell, $\hat{E}_\alpha^{(-)}(0,\tau)$ is the input negative-frequency field operator to the Raman cell, $\hat{Q}_\alpha^\dagger(z',0)$ is the initial atomic polarization operator at position z' and $\hat{F}_\alpha^\dagger(z',\tau')$ is a quantum Langevin operator needed to maintain operator consistency when collisional dephasing is included [24]. By comparing Eq. (A1) with Eq. (19), one can see that the second and fourth terms of Eq. (A1) correspond to the noise operator in Eq. (19). The kernels in Eq. (A1) are [16,24]

$$A_\alpha(z,z',\tau)=-i\kappa_2 E_{p\alpha}(\tau)e^{-\Gamma\tau}I_0([4\kappa_1\kappa_2(z-z')p_\alpha(\tau)]^{1/2})\ , \tag{A2}$$

$$B_\alpha(z,\tau,\tau')=(\kappa_1\kappa_2 z)^{1/2}E_{p\alpha}(\tau)e^{-\Gamma(\tau-\tau')}E_{p\alpha}^*(\tau')\frac{I_1(\{4\kappa_1\kappa_2 z[p_\alpha(\tau)-p_\alpha(\tau')]\}^{1/2})}{[p_\alpha(\tau)-p_\alpha(\tau')]^{1/2}}\ , \tag{A3}$$

$$C_\alpha(z,z',\tau,\tau')=-i\kappa_2 E_{p\alpha}(\tau)e^{-\Gamma(\tau-\tau')}I_0(\{4\kappa_1\kappa_2(z-z')[p_\alpha(\tau)-p_\alpha(\tau')]\}^{1/2})\ . \tag{A4}$$

Here κ_1 and κ_2 are constants that depend on the strengths of the transitions [30], Γ is the Raman-medium dephasing rate, z is the coordinate labeling the position along the pumped, pencil-shaped region of the Raman medium, τ is the retarded time ($\tau=t-z/c$), and I_0 and I_1 are modified Bessel functions. $E_{p\alpha}(\tau)$ is the classically treated pump field (assumed to be large) and $p_\alpha(\tau)$ is defined by

$$p_\alpha(\tau)\equiv\int_0^\tau|E_{p\alpha}(\tau'')|^2 d\tau''\ .$$

In our analysis we normally order the field operators to calculate the expectation value of the intensity pattern. With this ordering the only nonzero noise-operator correlation functions are

$$\langle\hat{Q}_\alpha^\dagger(z',0)\hat{Q}_\beta(z'',0)\rangle=(AN)^{-1}\delta(z'-z'')\delta_{\alpha,\beta}\ , \tag{A5}$$

$$\langle\hat{F}_\alpha^\dagger(z',\tau')\hat{F}_\beta(z'',\tau'')\rangle=\frac{2\Gamma}{AN}\delta(z'-z'')\delta(\tau'-\tau'')\delta_{\alpha,\beta}\ . \tag{A6}$$

Here A is the cross-sectional area of the pencil-shaped region pumped in the Raman cell and N is the density of molecules in the Raman medium. Equation (A5) states that the initial polarization fluctuations at one location in

the Raman medium are uncorrelated with the polarization fluctuations at another location. Similarly, Eq. (A6) states that the quantum-statistical collisional effects in the medium are uncorrelated position to position and time to time. The Kroneker δ functions simply indicate that these fluctuations are also uncorrelated between different Raman amplifiers, as one would expect. Recall that the noise operators in the ideal, single-mode, linear amplifier were also uncorrelated between different amplifiers.

The antinormally ordered correlation functions of the operators governing the growth of the noise are

$$\langle \hat{Q}_\alpha(z,0)\hat{Q}^\dagger_\beta(z',0)\rangle = 0 , \tag{A7}$$

$$\langle \hat{F}_\alpha(z',\tau')\hat{F}^\dagger_\beta(z'',\tau'')\rangle = 0 . \tag{A8}$$

One can see that Eqs. (A7) and (A8) lead to the result [Eq. (20)] that the expectation value of the antinormally ordered noise operator given in Eq. (19) is 0. As was noted in the text, these results assume that the Raman medium remains primarily in its ground state throughout the interaction with the radiation fields.

In the analysis presented in the discussion above, the derivation of the expressions for the visibility were for the ideal Mach-Zender interferometer presented in Fig. 1. Here we present the fairly straightforward changes in the formalism needed to model the experiment diagramed in Fig. 3.

Since the interferometer shown in Fig. 3 is nearly cyclic, both beam paths experience most of the optics in the interferometer, which makes the interferometer fairly insensitive to vibrations and thermal variations. Additional beam splitters, which we refer to as "pickoffs," allowed easy beam manipulation, but also led to a loss of signal input to the amplifiers that needed to be accounted for. Another loss of signal that needed to be included in the formalism came from the optics necessary for beam alignment between the generator and interferometer. The loss from these optics was treated as an attenuation beam splitter between the generator and interferometer. Including the losses from the beam splitters into the formalism for calculating the total output field from the interferometer gives

$$\hat{E}^{(-)}_{\rm tot}(x,\tau) = t_0 r_{p1}\hat{E}^{(-)}_{\rm I}(L,\tau) + r_0 r_{p2}\hat{E}^{(-)}_{\rm II}(L,\tau)e^{i\phi(x)} , \tag{A9}$$

where r_{p1} (r_{p2}) is the reflection coefficient of the pickoff optic in front of the upper (lower) amplifier in Fig. 3. Similarly, the input field to the upper (lower) amplifier is found to be $t_A r_i t_{p1}\hat{E}^{(-)}_G(L_G,\tau)$ [$t_A t_i t_{p2}\hat{E}^{(-)}_G(L_G,\tau)$] where t_{p1} [t_{p2}] is the transmission coefficient of the pickoff optic in front of the upper (lower) amplifier and t_A is the transmission coefficient that accounts for the loss between the generator and interferometer. All the beam-splitter coefficients are assumed to be constant across the Raman linewidth. Thus the inclusion of the extra optics affects the output fields only by scale factors.

Using normal ordering, the visibility was derived as indicated in Sec. III to get

$$V_{\rm pulse} = \frac{r_{p2}r_{p1}r_0 t_0\left[\int_{\rm pulse}\langle \hat{E}^{(-)}_{\rm I}(L,\tau)\hat{E}^{(+)}_{\rm II}(L,\tau)\rangle d\tau + \int_{\rm pulse}\langle \hat{E}^{(-)}_{\rm II}(L,\tau)\hat{E}^{(+)}_{\rm I}(L,\tau)\rangle d\tau\right]}{r_{p2}r_0^2\int_{\rm pulse}\langle \hat{E}^{(-)}_{\rm I}(L,\tau)\hat{E}^{(+)}_{\rm I}(L,\tau)\rangle d\tau + r_{p1}^2 t_0^2\int_{\rm pulse}\langle \hat{E}^{(-)}_{\rm II}(L,\tau)\hat{E}^{(+)}_{\rm II}(L,\tau)\rangle d\tau} . \tag{A10}$$

Inserting the full expressions for the amplified and generator fields as given in Eq. (A1) into Eq. (A10) leads to a plethora of terms that need to be evaluated to find the visibility. Since there are no serious complications involved in the evaluation of Eq. (A10) when the full expression for the Stokes field is inserted and because the calculation is rather arduous, the details will not be given here.

The calculation of the visibility is reduced to the evaluation of several integrals. The integrations over the spatial coordinate can be done analytically [32], but in general, numerical techniques are required for the temporal integrations.

To obtain quantitative predictions using the above formulas, the additional parameters listed below are needed. The effective cross-sectional area pumped by the pump laser was calculated [14] to be 4.25×10^{-3} cm^2, and the effective length of the Raman generator (amplifiers) was (were) calculated to be 1665 cm (1860 cm) [14]. To model the high gain in the amplifiers in the interferometer, the pump energy input to the amplifiers was taken to be approximately 0.37 mJ. The plane-wave gain coefficient [27] ($\alpha = 2.5\times10^{-9}$ cm/W) was used to calculate [30] the coupling constants.

[1] C. M. Caves, Phys. Rev. D **26**, 1817 (1982).
[2] R. J. Glauber, in *Frontiers in Quantum Optics*, edited by E. R. Pike and S. Sarkar (Hilger, London, 1986).
[3] H. A. Haus and J. A. Mullen, Phys. Rev. **128**, 2407 (1962).
[4] S. Stenholm, Phys. Scr. **T12**, 56 (1986).
[5] See, for a review, J. Clarke, IEEE Trans. Electron Devices **ED-27**, 1896 (1980).
[6] M. W. Cromar and P. Carelli, Appl. Phys. Lett. **38**, 723 (1981).
[7] R. A. Paananen, H. Statz, D. L. Bobroff, and A. Adams, Jr., Appl. Phys. Lett. **4**, 149 (1964).
[8] J. W. Kluver, J. Appl. Phys. **37**, 2987 (1966).
[9] T. A. Dorschner, H. A. Haus, M. Holz, I. W. Smith, and H. Stantz, IEEE J. Quantum Electron. **QE-16**, 1376

(1980).
[10] See, for example, M. Yamada, M. Shiumizu, M. Okayasu, T. Takeshita, M. Horiguchi, Y. Tachikawa, and E. Sugita, IEEE Photon. Technol. Lett. **2**, 295 (1990).
[11] O. V. Kulagin, G. A. Pasmanik, and A. A. Shilov, Kvant. Elektron. (Moscow) **17**, 355 (1990) [Sov. J. Quantum Electron. **20**, 292 (1990)].
[12] See, for example, I. A. Walmsley and M. G. Raymer, Phys. Rev. A **33**, 382 (1986).
[13] See, for example, N. Fabricius, K. Nattermann, and D. van der Linde, Phys. Rev. Lett. **52**, 113 (1984).
[14] See, for example, D. C. MacPherson, R. C. Swanson, and J. L. Carlsten, IEEE J. Quantum Electron. **QE-25**, 1741 (1989).
[15] J. Mostowski and M. G. Raymer, Opt. Commun. **36**, 237 (1981).
[16] M. G. Raymer and J. Mostowski, Phys. Rev. A **24**, 1980 (1981).
[17] M. D. Duncan, R. Mahon, L. L. Tankersley, and J. Reintjes, J. Opt. Soc. Am. B **7**, 1336 (1990).
[18] R. C. Swanson, P. R. Battle, and J. L. Carlsten, Phys. Rev. Lett. **67**, 38 (1991).
[19] See, for example, S. Friberg and L. Mandel, Opt. Commun. **46**, 141 (1983), and Refs. [2–5] therein.
[20] In our analysis we have chosen to normally order the field operators. Using this ordering, the degradation of the quantity of interest (visibility) will be seen to result wholly from amplified spontaneous emission in the amplifier. Consequently, we will refer to the amplified spontaneous emission as "noise." It should be noted that when the input field is in a minimum uncertainty state, the noise is equivalent to the mean-square fluctuation in the output mode as discussed in Ref. [1] minus $\frac{1}{2}$ quantum. The difference of $\frac{1}{2}$ quantum is insignificant at high gains and is a consequence of the difference in operator ordering between this work and Ref. [1].
[21] S. J. Kuo, D. T. Smithy, and M. G. Raymer, Phys. Rev. A **43**, 4083 (1991).
[22] (a) Glauber [2] has noted that a similar effect would be expected from a Young's double-slit experiment with an amplifier behind each slit. In fact, this experiment closely resembles Glauber's gedanken experiment; (b) for a more involved calculation of the visibility from an interferometer with amplifiers in each leg, see N. Hussain and R. Loudon, J. Mod. Opt. **36**, 1671 (1989).
[23] S. Prasad, M. O. Scully, and W. Martienssen, Opt. Commun. **62**, 139 (1987).
[24] M. G. Raymer in I. A. Walmsley, *Progress in Optics* (Elsevier, Amsterdam, 1990), Vol. 28, p. 181.
[25] P. R. Battle, R. C. Swanson, and J. L. Carlsten, Phys. Rev. A **44**, 1922 (1991).
[26] It is well known that high inversion leads to low noise. See, for example, A. Yariv, *Quantum Electronics,* 2nd ed. (Wiley, New York, 1975), p. 293.
[27] W. K. Bischel and M. J. Dyer, J. Opt. Soc. Am. B **6**, 677 (1986).
[28] The beam splitters were taken to have a transmission-to-reflection coefficient ratio of 50:50 for the purposes of calculating the average number of photons input to each amplifier. In fact, this is an overestimation for one amplifier and an underestimation for the other.
[29] K. Rzazewski, M. Lewenstein, and M. G. Raymer, Opt. Commun. **43**, 451 (1982).
[30] One should note the coupling constant product $\kappa_1\kappa_2$ in the fully quantum-mechanical theory [16,24] is 4 times larger than in the semiclassical theory [14,31].
[31] M. G. Raymer, J. Mostowski, and J. L. Carlsten, Phys. Rev. A **19**, 2304 (1979).
[32] *Handbook of Mathematical Functions,* edited by M. Abramowitz and I. Stegun (Dover, New York, 1965), Eqs. 11.3.31 and 11.3.29.